Static structure factor of polymerlike micelles: Overall dimension, flexibility, and local properties of lecithin reverse micelles in deuterated isooctane

Götz Jerke,[1] Jan Skov Pedersen,[2,*] Stefan Ulrich Egelhaaf,[3] and Peter Schurtenberger[1,*]
[1]*Institut für Polymere, ETH Zürich, CH-8092 Zürich, Switzerland*
[2]*Department of Solid State Physics, Risø National Laboratory, DK-4000 Roskilde, Denmark*
[3]*Institut Laue-Langevin, Large Scale Structures Group, Boîte Postale 156, F-38042 Grenoble, France*
(Received 1 April 1997)

We report a systematic investigation of the static structure factor $S(q,c)$ of polymerlike reverse micelles formed by soybean lecithin and trace amounts of water in deuterated isooctane using small-angle neutron scattering and static light scattering. The experimental data for different concentrations in the dilute and semidilute regime cover approximately three decades of scattering vectors. The data have been analyzed using polymer renormalization-group theory and a nonlinear least-squares fitting procedure based upon a numerical expression for the single chain scattering function of a wormlike chain with excluded-volume effects. Furthermore, the influence of interaction effects on the static structure factor have been successfully examined within a modified random-phase approximation. Additional information on the local scale has been extracted by applying indirect Fourier transformation and square-root deconvolution techniques. We demonstrate that we can determine structural properties such as the micellar cross-section profile and flexibility as well as quantitatively incorporate the influence of micellar growth and excluded-volume effects on $S(q,c)$.
[S1063-651X(97)11211-9]

PACS number(s): 82.70.Dd, 83.70.Hq, 61.12.Ex, 78.35.+c

I. INTRODUCTION

Surfactants in solution show a large variety of different microstructures with a structural evolution sensitive to control parameters such as temperature, concentration, or ionic strength. The morphology sequence of self-assembling systems is primarily determined by local geometrical constraints and a subtle balance of opposing forces originating from the polar head group and the hydrophobic tail region of the surfactant molecule. Several theoretical concepts have been formulated, which provide a link between microstructures and phase behavior based on concepts such as the spontaneous curvature [1–3] or the so-called packing parameter [4–6].

Among the different microstructures, wormlike aggregates have attracted widespread attention over the past two decades because these systems can serve as a prime example of equilibrium polymers. The term ''equilibrium'' or ''living polymer'' is used in a general sense for reversibly assembling linear objects. The equilibrium properties of these supramolecular aggregates strongly depend on concentration of self-assembling monomers and temperature [7,8]. Due to their transient nature, equilibrium polymers exhibit novel static and dynamic properties on time scales both long and short compared to their finite lifetime (for reviews see, for example, [9–15]). The obvious structural analogy between these systems and classical polymers has suggested that a deeper understanding of polymerlike micelles and microemulsions can be achieved by applying theoretical concepts from polymer physics. The one-dimensional growth of spherical micelles to elongated polymerlike aggregates has been observed in numerous aqueous surfactant systems upon a reduction of the spontaneous curvature through a variation of ionic strength (in ionic surfactant systems), temperature (in nonionic systems), or cosurfactant concentration [16–40], whereas in organic solvents polymerlike properties have been reported so far only in a few systems [41–49].

Despite the considerable experimental and theoretical attention given to the characterization and understanding of polymerlike micelles and microemulsions, precise knowledge of the micellar growth, flexibility, and structure as very important fundamental properties is still lacking. For example, it is usually accepted that for highly screened ionic surfactants or nonionic surfactants the weight-average micellar length $\langle L\rangle_w$ increases with a simple power law of the form $\langle L\rangle_w \sim c^{1/2}$ (or with $\langle L\rangle_w \sim c^{0.6}$ in the semidilute regime) [9]. Even though this is generally assumed, there is a surprising lack of solid data that supports it over a sufficiently large range of concentrations in surfactant solutions that indeed exhibit extensive micellar growth and the formation of giant wormlike micelles. This can be explained in part by the fact that the only practical method of quantitatively determining the micellar size in systems that form giant polymerlike micelles at low concentrations are scattering experiments. Any attempt to obtain the size distribution of anisotropic micelles is, however, severely hampered by the difficult task of distinguishing between the contributions from intermicellar interactions and concentration-dependent micellar growth to the scattering data.

Another aspect of wormlike micelles where we still lack detailed and quantitative information is the flexibility of the micelles as a function of micellar composition, ionic strength, or temperature. The flexibility l_p or bending modulus κ (which are related for one-dimensional objects via the thermal energy k_BT through $l_p=\kappa/k_BT$) are key parameters in a more fundamental description of fluid membrane phases

*Authors to whom correspondence should be addressed.

provided by the flexible surface model [50] and are crucial in any attempt to understand transitions such as the isotropic-to-nematic transition in micellar systems. Despite this fact there is only limited data available. Previous attempts have either relied on the use of simple crossover relations for the incorporation of flexibility in the intermediate-q range of data from small-angle neutron scattering (SANS) experiments [37,46] or alternatively used static light scattering (SLS) [51] or a combination of (SLS) and dynamic light scattering (DLS) together with polymer models such as the wormlike chain model in order to extract the persistence length [38,52–54]. However, both the influence of excluded-volume effects [54] and the incorporation of intermicellar interactions in the intermediate-q range are usually not included in the interpretation of scattering data. While it is generally believed that interaction effects do not affect the data at intermediate values of q, we demonstrate in this article that these effects indeed strongly influence the determination of l_p. It is clear from this that major progress in the interpretation of scattering experiments and a subsequent improvement in the understanding of the static and dynamic properties of equilibrium polymers based on scattering data requires a much more complete understanding of the static structure factor $S(q,c)$. This is still an unresolved problem mainly because of the difficulties that are encountered in an unambiguous differentiation between the effects of concentration-induced micellar growth and intermicellar interactions on $S(q,c)$ over a wide range of scattering vectors. A decoupling of micellar growth and intermicellar interaction effects has been achieved in the limit $q\rightarrow 0$. In several previous studies it has been demonstrated that one can clearly distinguish between the concentration-induced micellar growth and intermicellar interaction effects by combining results from polymer renormalization-group theory with a concentration-dependent micellar growth that results in an exponential size distribution of the micelles [40,55,56]. Following this procedure, a number of experimentally accessible quantities such as the osmotic compressibility (which is connected to the apparent molar mass M_{app}) and the static correlation length directly obey the same universal scaling laws as do classical polymers [40,56].

However, a complete incorporation of micelle formation and intermicellar interactions in a description of $S(q,c)$ over many decades of q remains a formidable and as yet incompleted task. Up to now the analysis of scattering data of polymerlike micelles relied generally on an interpretation of different q regimes based on asymptotic expressions such as the Guinier approximation for the low-q regime [57,58] and by considering crossover relationships for the incorporation of flexibility in the intermediate-q range [37,46]. Such a procedure provides only semiquantitative results because crossover transitions are not always as pronounced as they should be for a reliable determination of physical properties such as the flexibility. Moreover, such an analysis uses only part of the information that is contained in the experimental data. Therefore, a major improvement is the application of a least-squares analysis with a suitably parametrized model cross section [39]. Until recently, we were facing the problem that even for the case of dilute solutions without intermicellar interactions no suitable scattering functions of wormlike chains with excluded-volume effects were available that cover the crossover from rod to coil behavior and span several decades in the q range. This shortcoming has been overcome by a recently conducted series of Monte Carlo simulations where excluded-volume effects have explicitly been incorporated [59]. The model used in the off-lattice Monte Carlo simulation studies is a discrete representation of the wormlike chain model developed by Porod and Kratky [60,61]. The calculated single-chain scattering functions have been parametrized according to the approach by Yoshizaki and Yamakawa [62], so that a least-squares analysis is now feasible [63].

In the present study we focus our attention on the fundamental problem of obtaining quantitative information on micellar growth, flexibility, and structure. We have conducted several series of extended SANS measurements of reverse micellar solutions of lecithin in deuterated isooctane, which are complemented by a careful light scattering study. The combined data sets contain structural information over an extended q range of approximately three decades for a series of surfactant concentrations below and above the overlap threshold. Considerable effort has already been devoted previously to the characterization of polymerlike reverse micelles of lecithin in a variety of different organic solvents using techniques such as SLS, DLS [54–56,64], and SANS [44–46,65] and with rheological measurements [43,44]. Based on these studies, the following picture emerged. The micellar size is strongly dependent on both the water content and the surfactant concentration. At low water content, the micelles are found to be quite small and the solutions exhibit static and dynamic properties that are typical for colloidal solutions. Upon further addition of water, the micelles become giant and resemble semiflexible polymers in solution and they can form entanglement networks at concentrations above the so-called entanglement threshold or overlap concentration c^*. In this study we use this model system in order to make the next step towards a quantitative understanding of the structural properties of equilibrium polymers.

We present an analysis of the scattering data, which uses the well-established renormalization-group theory approach to extract the growth behavior of the overall properties, whereas the analysis of the properties on intermediate length scales are based on the nonlinear least-squares fitting procedure, which incorporates polydispersity effects and explicitly takes into account the local tubular cross section of the micelles. In addition, on the local length scale the geometrical model of a flexible but locally stiff and tubular structure has been confirmed in SANS contrast variation experiments where the inner H_2O core was exchanged with D_2O. This investigation is in direct analogy to former theoretical and experimental studies where we analyzed the local structure of polymerlike lecithin reverse micelles in deuterated cyclohexane [66,67]. Finally, we made an attempt to achieve a self-consistent description of both micellar growth and interaction effects on the entire $S(q,c)$ by using the results from a recent Monte Carlo simulation study of many-chain systems that has suggested that a modified random-phase approximation can be used [68].

II. MATERIAL AND METHODS

A. Materials and sample preparation

Soybean lecithin was obtained from Lucas Meyer (Epikuron 200) and used without further purification. Fully deuter-

ated isooctane-d_{18} (98% purity, 2,2,4-trimethylpentane) was purchased from Cambridge Isotope Laboratories. The water used was purified with a Milli-Q water purification system from Millipore. Samples were prepared as follows. First lecithin was dissolved in deuterated isooctane for approximately 16 h using a magnetic stirrer and then water was added with a microliter syringe (Hamilton) under stirring. Complete mixing was achieved by gentle stirring for a few hours. The samples were finally equilibrated for a few days in the dark at 26 °C. The concentration series for SLS measurements were done step by step by serial dilution from a 15.88-mg/ml stock solution [69].

B. Methods

1. Static light scattering

Static light scattering experiments were made with a fiber optical setup based upon a Malvern PS/MW spectrometer, equipped with an argon ion laser (Coherent, Innova 70, $\lambda_0 = 488$ nm) and a computer-controlled and stepping-motor-driven variable detection system. Measurements were usually performed at a temperature of 26 °C±0.2 °C. Approximately 1 ml of the solution was transferred into the cylindrical scattering cell (10 mm diameter). The scattering cell was then stoppered and centrifuged for approximately 30 min at 5000 g and 26 °C in order to remove dust particles from the scattering volume. Experiments were performed at 35 different angles between ($15.2° \leqslant \theta \leqslant 145°$) and 30–60 individual measurements were taken and averaged for each angle. The data were then corrected for background (cell and solvent) scattering and converted into absolute scattered intensities $d\sigma(\theta)/d\Omega$ using toluene as a reference standard. The absolute scattered intensity per volume was calculated using [70]

$$\frac{d\sigma}{d\Omega}(\theta) = \frac{\Delta\langle I(\theta)\rangle}{\langle I_{\mathrm{ref}}(\theta)\rangle}\left(\frac{d\sigma}{d\Omega}\right)_{\mathrm{ref}}\left(\frac{n}{n_{\mathrm{ref}}}\right)^2, \tag{1}$$

where $\Delta\langle I(\theta)\rangle$ and $\langle I_{\mathrm{ref}}(\theta)\rangle$ are the average scattered intensity of the solution and the average scattered intensity of the reference solvent toluene, $(d\sigma/d\Omega)_{\mathrm{ref}} = 39.6\times10^{-4}\ \mathrm{m}^{-1}$ is the absolute scattered intensity of toluene (per volume), and n and n_{ref} are the index of refraction of the solution and the reference solvent, respectively. The apparent molar mass M_{app} and the static correlation length ξ_s were determined from the intercept and slope of a plot of $cK_{\mathrm{SLS}}/d\sigma(q)/d\Omega$ versus q^2 using a Lorentzian scattering law of the form

$$\frac{cK_{\mathrm{SLS}}}{\frac{d\sigma}{d\Omega}(q)} = \frac{1}{M_{\mathrm{app}}}(1+q^2\xi_s^2), \tag{2}$$

where $q = (4\pi n/\lambda_0)\sin(\theta/2)$ is the magnitude of the scattering vector. In the limit $c\to0$ the correlation length ξ_s is connected to the z average of the radius of gyration $\langle R_{g,0}\rangle_z$ via $\xi_s^2 = \frac{1}{3}\langle R_{g,0}^2\rangle_z$, where $R_{g,0}$ is the root-mean-square radius of gyration of a single coil. The contrast term is given by

$$K_{\mathrm{SLS}} := \frac{4\pi^2 n^2}{N_A\lambda_0^4}\left(\frac{dn}{dc}\right)^2, \tag{3}$$

where dn/dc is the refractive index increment (with $dn/dc = 9.307\times10^{-5}\ \mathrm{m}^3/\mathrm{kg}$ for $w_0 = 1.5$), c is the surfactant concentration plus water, and N_A is the Avogadro number.

The accessible range of scattering angles results in $4.7\times10^{-4}\ \text{Å}^{-1} \leqslant q \leqslant 3.4\times10^{-3}\ \text{Å}^{-1}$. The fit range was restricted to scattering angles of $15.2° \leqslant \theta \leqslant 47.7°$ so that only the low-q part was included in the fit, for which we can use the approximation given in Eq. (2).

2. Small-angle neutron scattering

The small-angle neutron scattering experiments were partly performed at the SANS facility installed at the DR3 reactor of the Risø National Laboratory, Denmark. An extended range of scattering vectors from $3.7\times10^{-3}\ \text{Å}^{-1} \leqslant q \leqslant 0.45\ \text{Å}^{-1}$ was covered by four combinations of neutron wavelength ($\lambda = 3.5$ and 10 Å) and sample-to-detector distances ($d = 1-6$ m). The wavelength resolution was 18% (full width at half maximum value).

Further SANS measurements with identical samples for a cross-check and with additional concentration series have been done at the D22 instrument of the Institut Laue Langevin (ILL), France [71]. The experiments at ILL allowed us to extend the q range to lower values so that a significant overlap between SANS and SLS data could be obtained. Furthermore, low-concentration samples have been measured within reasonable time because of the high neutron flux rate. An extended range of scattering vectors $1.8\times10^{-3}\ \text{Å}^{-1} \leqslant q \leqslant 0.32\ \text{Å}^{-1}$ was covered by three combinations of neutron wavelength ($\lambda = 6.2$ and 18 Å; in a further run $\lambda = 9$ and 12 Å) and sample-to-detector distances ($d = 1.4-17.9$ m). All experiments at D22 were done with a 40-cm detector offset. The wavelength resolution was 10% (full width at half maximum value).

The samples were kept in stoppered quartz cells (Hellma, Germany) with a path length of 2 mm. The neutron spectra of water used for calibration was measured with a 1-mm-path-length quartz cell. The raw spectra were corrected for background from the solvent, sample cell, and electronic noise by conventional procedures. Furthermore, the two-dimensional isotropic scattering spectra were azimuthally averaged, converted to absolute scale, and corrected for detector efficiency by dividing with the incoherent scattering spectra of pure water [72–75].

The average excess scattering length density per unit mass $\Delta\rho_m$ of the tubular reverse micelles in deuterated isooctane was determined from the known chemical composition of lecithin [76,77]. The corresponding values are $\Delta\rho_m^{\mathrm{head}} = -5.60\times10^{10}$ cm/g (lecithin headgroup), $\Delta\rho_m^{\mathrm{tail}} = -5.88\times10^{10}$ cm/g (lecithin tail), $\Delta\rho_m^{\mathrm{H_2O}} = -6.89\times10^{10}$ cm/g (water), and $\Delta\rho_m^{\mathrm{D_2O}} = 0.068\times10^{10}$ cm/g (deuterated water).

The smearing induced by the different instrumental setups is included in the data analysis discussed below. For each instrumental setting the ideal model scattering curves were smeared by the appropriate resolution function when the model scattering intensity was compared to the measured one by means of least-squares methods [78,79]. The parameters in the models were optimized by conventional least-squares analysis and the errors of the parameters were calculated by conventional methods [80].

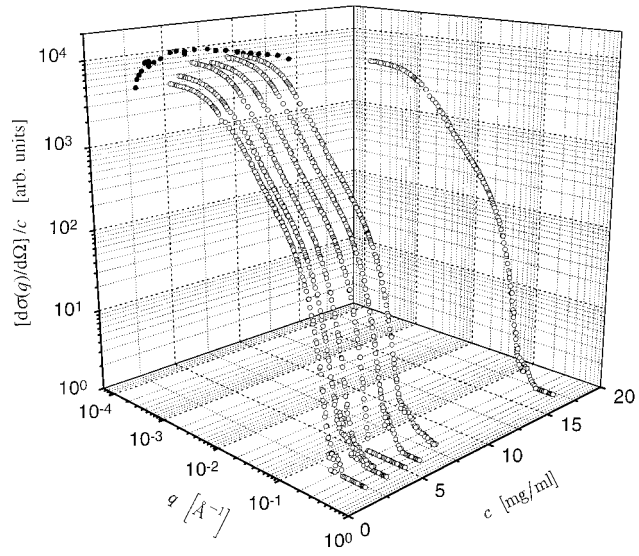

FIG. 1. Scattered intensity $[d\sigma(q)/d\Omega]/c$ versus scattering vector q and concentration c for lecithin reverse micelles in deuterated isooctane with a molar water-to-lecithin ratio of $w_0=1.5$. Data shown were obtained from SLS (low-q range) and SANS (intermediate and high-q range) measurements. In the limit $q\rightarrow 0$, the scattered intensity (given by ●) is mainly dominated by the concentration-induced micellar growth at low concentrations and by intermicellar interactions at high concentrations.

III. RESULTS AND DISCUSSION

A. General features

Figure 1 shows typical results of SLS and SANS experiments for the concentration and q dependence of the normalized scattered intensity $[d\sigma(q)/d\Omega]/c$ from lecithin reverse micelles in deuterated isooctane with a molar water-to-lecithin ratio $w_0=1.5$. It clearly demonstrates the extensive concentration-induced micellar growth, which is visible at low values of c, as well as the strong effect of intermicellar interactions, which dominate $[d\sigma(q)/d\Omega]/c$ at $c>c^*$. Figure 1 can also serve as a good example for the close analogy between giant wormlike micelles and semiflexible polymers in a good solvent.

For most equilibrium polymer systems the whole set of static properties is only accessible through a combination of SLS and SANS. Depending on the length scale, which is essentially given by $1/q$, structural information can be obtained about the overall dimensions, the flexibility, and the locally cylindrical cross section of the polymerlike micelles. While SLS experiments are ideally suitable for a determination of the overall size and apparent molar mass of large cylindrical micelles due to the restriction to low values of q, the flexibility and the local structure of the micelles has to be determined by SANS experiments. For classical polymers, one would expect to find the following three distinct regions in the scattering data. At low q, the Guinier region associated with the overall size of the chain (apparent molar mass M_{app} and static correlation length ξ_s) is observed. At slightly higher q, the scattered intensity of a single coil crosses over to a power-law behavior with an exponent of -2 in θ solvents and about $-\frac{5}{3}$ in good solvents. These exponents are characteristic of the random-walk and self-avoiding-walk configurations of the chain in θ and good solvents, respectively. At higher q, one probes shorter length scales and the local stiffness of the chain shows up as a crossover to a q^{-1} behavior. At even higher q the local cross-section structure of the chain gives rise to a cross-section Guinier behavior and a strong decrease in the scattered intensity. Such a behavior can indeed be observed for polymerlike micelles as shown in Fig. 1. The main difference between classical polymers and micelles arises from the concentration-induced micellar growth, which results in a pronounced increase of the forward scattered intensity with increasing concentration. However, this specific feature of equilibrium polymers becomes masked by intermicellar interactions at concentrations above the overlap threshold c^* and the typical features of an entanglement network of semiflexible polymers are recovered at $c>c^*$. As we will demonstrate later, there are nevertheless distinct differences between polymers and micelles even at $c>c^*$, which we can exploit in order to experimentally determine the growth exponent predicted by the theoretical models of micelle formation.

As discussed in the Introduction, reverse micellar solutions of lecithin in organic solvents not only exhibit a strong concentration dependence of the micellar size but they are also extremely sensitive to the amount of water added. It has previously been demonstrated that the addition of trace amounts of water induces considerable growth of the reverse micelles. This is also shown in Fig. 2(a), which presents the q dependence of the scattered intensity for two values of the lecithin-to-water ratio ($w_0=1.5$ and 2.5). The concentrations are in both cases comparable (2 and 2.5 mg/ml, respectively) and below c^*, i.e., the scattered intensity is dominated by single-particle properties and the effects of intermicellar interactions are small. We see that the forward scattered intensity (e.g., apparent molar mass and correlation length) increases significantly with increasing water content, whereas the local structure (e.g., mass per length and cross-section radius of gyration) remains almost unchanged, as will be demonstrated in detail later.

At $w_0=2.5$ the resulting polymerlike micelles are extremely large already at small values of c and the scattered intensity shows the various characteristic asymptotic regimes over a quite extended range of q. We have thus measured several samples of lecithin in isooctane with $w_0=2.5$ in order to demonstrate further the different concentration regimes more clearly. The corresponding experimental data are summarized in Fig. 2(b) for two different concentrations ($c_1=0.90$ mg/ml and $c_2=3.49$ mg/ml). The actual concentration values were chosen in such a way that one can follow the concentration induced growth at low concentrations ($c_1<c_2\approx c^*$).

B. Data analysis: Apparent molar mass

As pointed out in the Introduction, the analysis of the detailed structure and size distribution of anisotropic micelles is severely hampered by the difficult task of distinguishing between the contributions from intermicellar interactions and concentration-dependent micellar growth to the scattered intensity. This has been illustrated with Figs. 1 and 2(b). In the first step of our data evaluation we concentrate on the light scattering data obtained for $w_0=1.5$, i.e., we

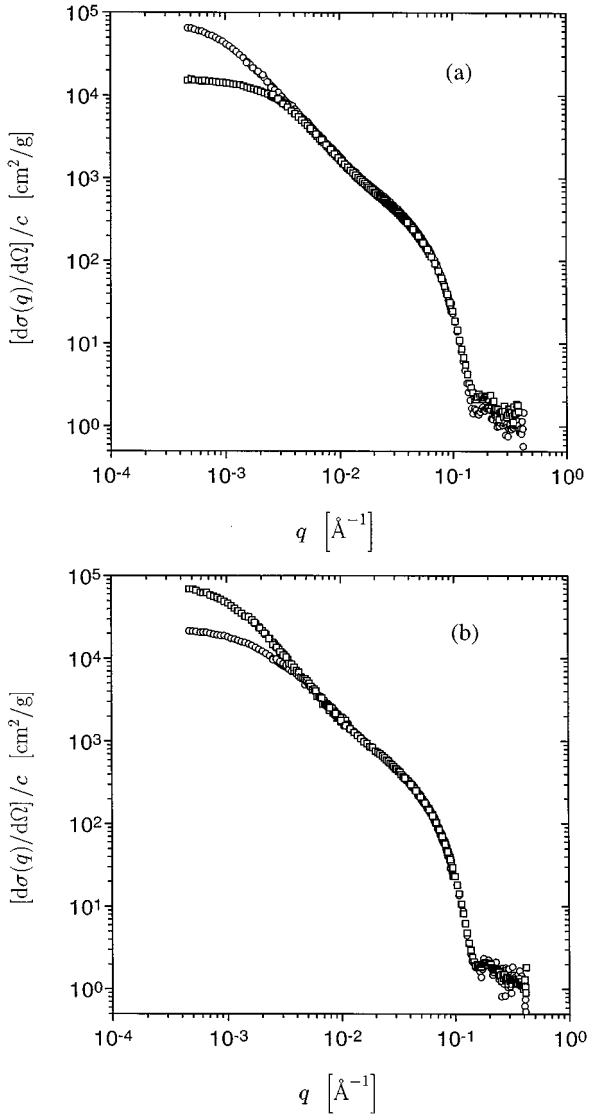

FIG. 2. Scattered intensity $[d\sigma(q)/d\Omega]/c$ of lecithin wormlike micelles in deuterated isooctane as a function of solution composition. (a) Comparison of two dilute samples with different water-to-lecithin ratios (□, $w_0=1.5$; ○, $w_0=2.5$), but similar concentrations ($c=2$ and 2.5 mg/ml, respectively) reveals that micelles with a higher water content show a much more pronounced growth behavior. (b) Characteristic q dependence of the scattered intensity, for samples with a fixed water-to-lecithin ratio $w_0=2.5$ for two different lecithin concentrations below (○, $c_1=0.90$ mg/ml) and approximately at (□, $c_2=3.49$ mg/ml) the overlap threshold c^*.

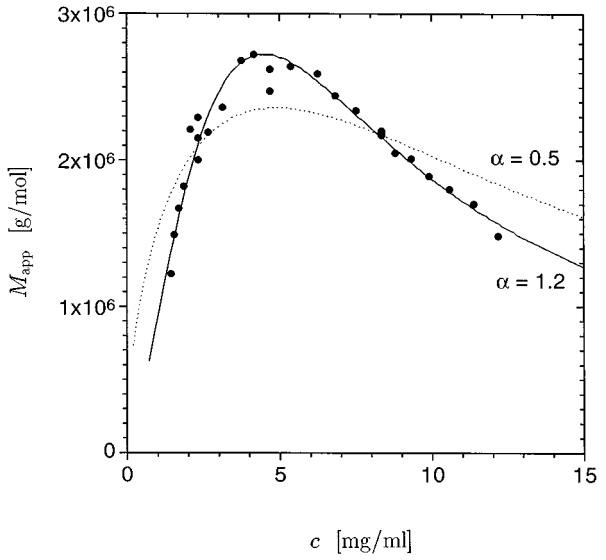

FIG. 3. Apparent molar mass M_{app} versus concentration c for lecithin reverse micelles in deuterated isooctane at a water-to-lecithin ratio of $w_0=1.5$. Also shown is the best fit to the data according to the renormalization-group theory approach, which results in a growth exponent of $\alpha=1.23$ (solid line). A fit with a mean-field growth exponent of $\alpha=0.5$ (dotted line) shows the incompatibility of the data with the prediction of classical mean-field models.

focus our attention on a detailed evaluation of the initial part of the scattering curves given in Fig. 1. The experimental results for the concentration dependence of the apparent molar mass as obtained from SLS are summarized again in Fig. 3. We can try to analyze the concentration dependence of M_{app} by including both a concentration dependence of the micellar size given by a power law of the form $M\sim c^{\alpha}$ as well as a description of intermicellar interactions based on conformation space renormalization-group theory originally developed for semidilute polymer solutions [81]. Such an analysis previously has been applied to solutions of polymer-like reverse micelles and nonionic micelles and details can be found elsewhere [40,55]. In the limit of $q\to 0$ the scattered intensity is related to the molar mass M through

$$\frac{1}{cK_{SLS}}\frac{d\sigma}{d\Omega}(0)=\langle M\rangle_w S(0)=M_{app}, \tag{4}$$

where $S(0)$ is the static structure factor at $q=0$ and $\langle M\rangle_w$ is the weight-average molar mass [82]. For polymers, $S(0)=f(X)$ can be written as a function of a reduced concentration X, which is proportional to the concentration, the osmotic second virial coefficient, and the molar mass. For monodisperse polymers, one finds $X=\frac{16}{9}A_2cM$ and the osmotic second virial coefficient A_2 is given by

$$A_2\approx 4\pi^{3/2}N_A\frac{\overline{R_{g,0}^3}}{M^2}\Psi, \tag{5}$$

where Ψ is the degree of interpenetration in dilute solution and $R_{g,0}$ is the root-mean-square radius of gyration of a single coil [83]. Polydispersity can be accounted for by using [100]

$$X=\frac{A_2c\langle M\rangle_w}{\frac{9}{16}-\frac{1}{8}\ln\frac{\langle M\rangle_w}{\langle M\rangle_n}}, \tag{6}$$

where $\langle M\rangle_w$ and $\langle M\rangle_n$ are the weight- and number-averaged molar mass of the polymer, respectively. In our analysis we apply the commonly used Schulz-Zimm distribution [84,85]

$$N(M)=\frac{M^z}{z!}\left(\frac{z+1}{\langle M\rangle_n}\right)^{z+1}e^{-M(z+1)/\langle M\rangle_n}. \tag{7}$$

The parameter z is related to the polydispersity index σ^2 by $\sigma^2=1/(z+1)$. We fixed the polydispersity to $\langle M\rangle_w/\langle M\rangle_n=2$, which results in $z=1$ [9]. An explicit functional form

for $S(0)$, for example, has been calculated using the renormalization-group method [86]

$$S(0)^{-1}=1+\frac{1}{8}\left(9X-2+\frac{2\ln(1+X)}{X}\right)\times\exp\left\{\frac{1}{4}\left[\frac{1}{X}+\left(1-\frac{1}{X^2}\right)\ln(1+X)\right]\right\} \quad (8)$$

and good agreement between theory and light scattering data was found for classical polymers with different values of $\langle M\rangle_w$ for an extended range of concentrations $10^{-2}<X<10^2$ [87]. A major problem in a direct application of polymer theory to lecithin reverse micelles comes from the concentration dependence of the micellar size distribution. Since A_2 depends on c, we incorporate a power law of the form

$$\langle M\rangle_w=B_1c^{\alpha} \quad (9)$$

and a scaling law of the form $\overline{R_g}\sim M^{\nu}$ in the relations for A_2 in Eq. (5). This leads to $A_2\sim c^{\alpha(3\nu-2)}$, and according to Eq. (6) the reduced concentration X is then given by

$$X=2.1B_1^{(3\nu-1)}B_2c^{[\alpha(3\nu-1)+1]}, \quad (10)$$

where B_2 provides the link between A_2 and $\langle M\rangle_w$. Equations (9) and (10) allow an explicit description of the micellar features of an equilibrium size distribution in the renormalization-group treatment of $S(0)$ given by Eq. (8) [55]. As shown in Fig. 3, this allows a quantitative reproduction of the concentration dependence of the apparent molar mass. The resulting best-fit parameters using a nonlinear least-squares fitting routine are $\alpha=1.23\pm0.08$, $B_1=4.89\times10^9$ g$^{1-\alpha}$ ml$^{\alpha}$ mol^{-1}, and $B_2=6.60\times10^{-4}$ g$^{-3\nu}$ ml mol$^{3\nu-1}$, while the scaling exponent ν was kept fixed to the excluded-volume value of $\nu=0.588$ according to the results from previous light scattering measurements [54] and an analysis of SANS data at low concentrations. In the case of $w_0=2.5$ the corresponding values are $B_1=33.14\times10^9$ g$^{1-\alpha}$ ml$^{\alpha}$ mol^{-1}, and $B_2=3.23\times10^{-4}$ g$^{-3\nu}$ ml mol$^{3\nu-1}$ with $\alpha=1.23$ and $\nu=0.588$ fixed. It is important to point out that we once again obtain a very high growth exponent $\alpha=1.23\pm0.08$, which is in good agreement with the previously determined value of $\alpha=1.2\pm0.3$ for a similar organic system (cyclohexane instead of deuterated isooctane) [55] and of $\alpha=1.1\pm0.1$ for $C_{16}E_6$ in D_2O [40].

The incompatibility of the present data with a growth exponent according to the classical mean-field models for micellar growth is shown in Fig. 3, where we tried to fit the experimental data using a fixed growth exponent $\alpha=0.5$. Figure 3 in particular demonstrates that the actual value of α not only determines the initial slope of the c dependence of $M_{\rm app}$ but furthermore distinctly influences the region beyond c^*. This is a consequence of the fact that the value of A_2 (and thus c^*) is primarily given by the molar mass of the semiflexible chain. While A_2 therefore remains constant for classical polymers and the value of X is simply proportional to c, for equilibrium polymers this is not the case and X increases with a power law of the concentration. As a result, we can determine the concentration dependence of $M_{\rm app}$ much more precisely than originally believed since the forward scattering does not become insensitive to the micellar size in the semidilute regime and we do not have to rely on the experimental data obtained in the dilute regime only. This has in fact been overlooked in a previous attempt to use Eq. (8) in the interpretation of static light scattering data from the ionic surfactant hexadecyltrimethylammonium bromide at high ionic strength [88]. While Eq. (8) has been applied in order to incorporate interaction effects, c^* was used as a constant without allowing it to vary in response to the increasing micellar size. X was then calculated from the ratio c/c^*, i.e., assumed to increase linearly with concentration. We therefore believe that the reported good agreement between the experimentally determined forward scattering and the calculations based on the theoretical mean-field expectations, i.e., assuming $\alpha=\frac{1}{2}$, should be considered with caution [88]. A careful inspection of Fig. 15 in Ref. [88] indeed reveals good agreement between data points and theoretical curve at low concentrations, but also systematic deviations at and beyond c^* that are quite similar to those we find when using a too-small value of α (see Fig. 3).

At present we have no clear understanding of the large values of α that we have found in a number of different systems that form giant polymerlike micelles. For lecithin in isooctane the extent of the micellar growth can be finely tuned by the amount of water added. In a preliminary investigation under conditions where we already observe the formation of large polymerlike reverse micelles, but where the resulting sizes are considerably smaller than in the present study at similar surfactant concentrations, we indeed found a smaller growth exponent of $\alpha=0.63\pm0.05$ [89], in good agreement with mean-field predictions. As soon as we induced a more pronounced growth, as in, for example, the present study (Fig. 3), we encountered a situation that is totally incompatible with the predicted mean-field exponents. The hypothesis that the concentration dependence of the micellar size may be much more pronounced for giant polymerlike micelles is further supported by recent studies of micelle formation in nonionic surfactant systems. A careful series of static light scattering experiments performed with very dilute solutions of the nonionic surfactant $C_{12}E_6$ at different temperatures [90] demonstrates that slightly above the critical micellar concentration, the micellar aggregation number $N_{\rm agg}$ increases weakly with concentration and then crosses over to a power law of the form $N_{\rm agg}\sim c^{1/2}$, as predicted by the classical mean-field models of micelle formation. However, in a recent light scattering investigation [40] of another nonionic surfactant from the same class ($C_{16}E_6$), where giant wormlike micelles are formed, a value of $\alpha=1.1\pm0.1$ was found and it has been demonstrated that the data are clearly incompatible with a power-law exponent of $\frac{1}{2}$. It is clear from this that additional and careful investigations are required in which the extent of micellar growth is carefully adjusted.

C. Data analysis: Local structure

As we have seen from the data shown in Figs. 1–3, surfactant concentration has an enormous effect on the scattered intensity at low values of q as a result of the combined influences of micellar growth and intermicellar interactions. We have demonstrated in Fig. 3 that the contributions from growth and interactions can be successfully decoupled using

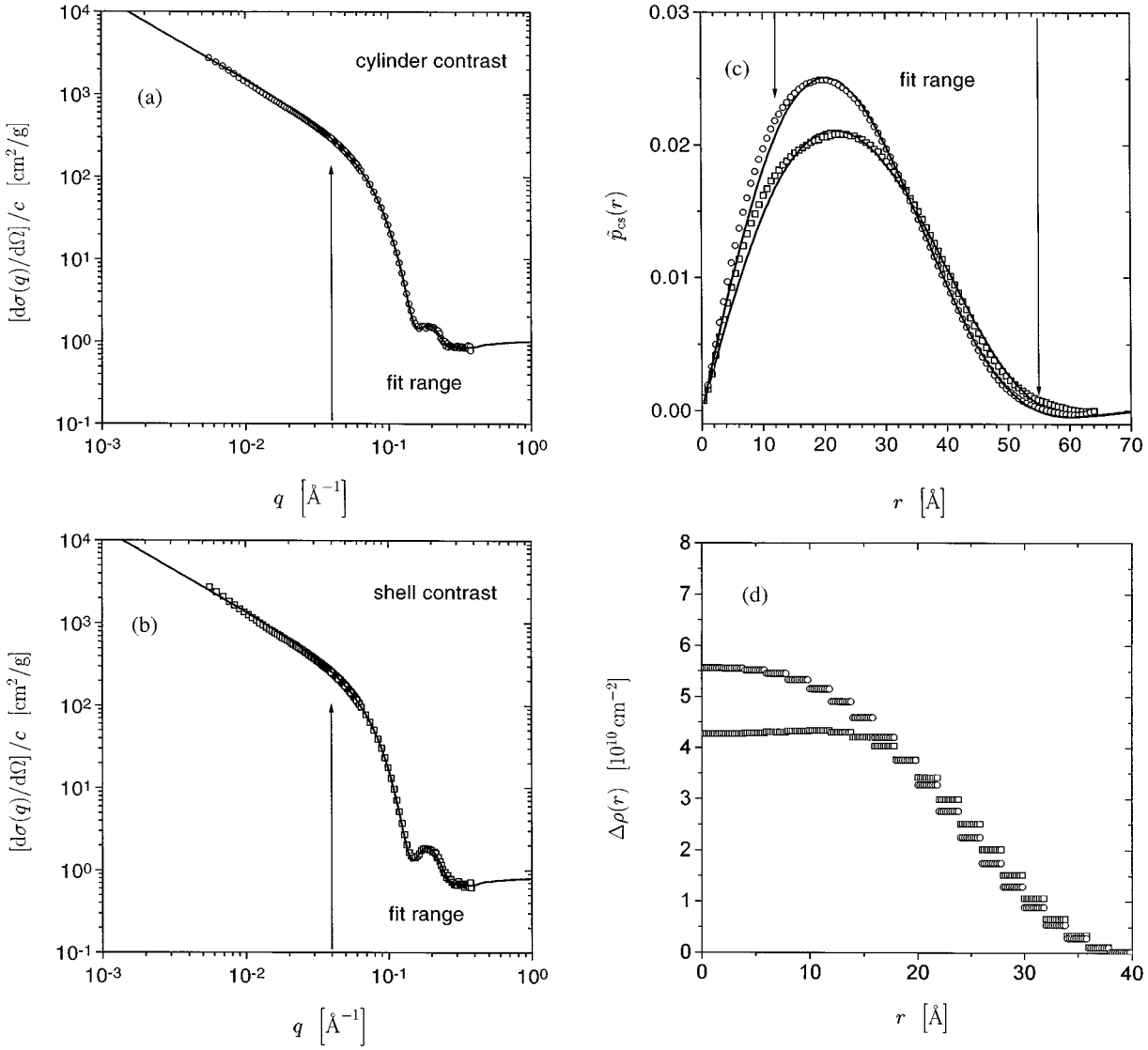

FIG. 4. (a) and (b) Comparison of the experimental (open symbols) and fitted $[d\sigma(q)/d\Omega]/c$ scattered intensity using the indirect Fourier transformation method for wormlike reverse micelles in deuterated isooctane at a molar water-to-lecithin ratio of $w_0=2.0$, (c) the corresponding distance distribution functions, and (d) the radial excess scattering length density profiles. (a) and (b) Scattered intensity versus q for reverse micellar samples with (a) H_2O (○, cylinder contrast) and (b) D_2O (□, shell contrast). Fits to the data are given as solid lines and the lower cutoff value of the q range used in the IFT is indicated with arrows. (c) Distance distribution function $\tilde{p}_{CS}(r)$ as determined by the IFT for reverse micellar samples with H_2O (○) and D_2O (□). Solid lines represent the fits in the range $12\,\text{Å} \leqslant r \leqslant 55\,\text{Å}$ (indicated by arrows) by a square-root deconvolution of $\tilde{p}_{CS}(r)$. (d) Calculated radial excess scattering length density profile $\Delta\rho(r)$ by deconvoluting $\tilde{p}_{CS}(r)$.

renormalization-group theory. In contrast to this, the data at high values of q, which primarily reveal details of the local structure, appear to be independent of concentration. This is a result of the fact that micellar growth occurs in a one-dimensional fashion along the micellar contour and leaves the cylindrical cross section unaltered and because intermicellar interactions are strongly screened on local length scales. Therefore, we can expect that an analysis of the scattered intensity using single-particle scattering functions in order to determine the micellar cross-section structure, and to a lesser degree flexibility, should result in good estimates. Since the mass per length and the micellar flexibility are important parameters in any attempt to link molar mass as determined from the forward scattering with micellar dimensions and structure, we thus continue with an analysis of the scattering data on local length scales.

As described in detail previously [66,67] we can extract information on the local structure of the reverse micelles by applying the indirect Fourier transformation (IFT) [91,92] and the square-root deconvolution (SQDEC) method [93] to the experimental data from the high-q regime. The locally cylindrical structure can be analyzed with a high degree of accuracy if we focus on a sample in the semidilute regime where the lecithin concentration is only slightly above the overlap threshold c^*. We have chosen a reverse micellar solution with a water-to-lecithin ratio of $w_0=2.0$ and a total weight concentration of lecithin plus water of $c=16$ mg/ml (see Fig. 4). In this special case we benefit from a high ratio

of coherent intensity to background, but we still work under conditions with a well-defined separation of length scales as required in the decoupling approximation used below [66]: The static correlation length ξ_s exceeds the apparent persistence length $l_{p,\mathrm{app}}$, which is again larger than the cross-section radius of gyration $R_{\mathrm{CS},g}$ of the tubular reverse micelles, $\xi_s > l_{p,\mathrm{app}} > R_{\mathrm{CS},g}$. Figures 4(a) and 4(b) show the q dependence of the scattered intensity for two different scattering contrasts used to investigate the local arrangement of surfactant and water. By using D_2O instead of H_2O we achieve a different labeling of our samples. Normal water and lecithin give rise to nearly the same scattering contrast against the deuterated solvent. Therefore, we expect to find the scattering pattern of a nearly homogeneous cylinder on the local length scale, whereas the samples with D_2O should look like hollow cylinders with a typical shell contrast, i.e., a much more pronounced first minimum for the cross-section form factor. This can be clearly seen in the scattering shown in Figs. 4(a) for cylinder and 4(b) for shell contrast [94].

On length scales where the scattered intensity is controlled by the local stiffness of the micelles, it is possible to decouple the data into two contributions: one that originates from the wormlike chain structure and another that reflects the local cylindrical cross-section structure [66,67]. Provided that $\xi_s > l_{p,\mathrm{app}} > R_{\mathrm{CS},g}$ the asymptotic behavior of the scattering function for $q > 1/l_{p,\mathrm{app}}$ can be expressed by

$$\frac{d\sigma}{d\Omega}(q) = \left(\frac{\pi}{q}\right) 2\pi \int_0^\infty \tilde{p}_{\mathrm{CS}}(r) J_0(qr)\, dr = \left(\frac{\pi}{q}\right) I_{\mathrm{CS}}(q), \tag{11}$$

where J_0 is the zeroth-order Bessel function and $I_{\mathrm{CS}}(q)$ the cross-section scattering intensity. This has been demonstrated in [66] for noninteracting wormlike cylinders and in [67] for lecithin reverse micelles in deuterated cyclohexane at $c > c^*$. The normalized cross-section distance distribution function $\tilde{p}_{\mathrm{CS}}(r)$ is given by

$$\tilde{p}_{\mathrm{CS}}(r) = \frac{2\pi c}{M_L} \int_0^\infty \Delta\rho(r')\Delta\rho(r+r')\, r'\, dr', \tag{12}$$

where M_L is the mass per length of the cylindrical micellar core. Note that $\tilde{p}_{\mathrm{CS}}(r)$ and $I_{\mathrm{CS}}(q)$ contain a factor c/M_L, which is important for absolute normalization of the data.

As described previously [66,67], we obtain a parametrized form of the distance distribution function $\tilde{p}_{\mathrm{CS}}$ by applying the IFT method. The resulting values of $\tilde{p}_{\mathrm{CS}}$ and a comparison of fitted and experimental values of the scattered intensity are shown in Fig. 4(c) for the data obtained from a sample in the semidilute regime $w_0 = 2.0$ (with $c = 16$ mg/ml). The lower limit $q_{\min} = 0.04\ \text{Å}^{-1}$ [indicated with arrows in Figs. 4(a) and 4(b)] of the fitted q range was chosen close to the limit where the crossover from stiff to flexible behavior occurs. Experimental data and fitted curves coincide perfectly within the fit range of $q \geq 0.04\ \text{Å}^{-1}$ and the expected strong deviations in the low-q regime due to the crossover from locally stiff to flexible coil structure are clearly visible.

TABLE I. Cross-section radius of gyration $\overline{R}_{\mathrm{CS},g}$, cross-section forward scattering intensity $I_{\mathrm{CS}}(0)$, and mass per unit length M_L obtained by the indirect Fourier transformation method for lecithin reverse micelles in deuterated isooctane ($w_0 = 2$, $c = 16$ mg/ml) with cylinder (H_2O) and shell (D_2O) contrast.

Contrast	$\overline{R}_{\mathrm{CS},g}$ (Å)	$I_{\mathrm{CS}}(0)$ (10^8 cm/g)	M_L (10^{-13} g/cm)
H_2O	18.3	5.15	1.52
D_2O	19.2	4.43	1.45

Having determined $\tilde{p}_{\mathrm{CS}}(r)$, we are able to calculate integral parameters of the micellar cross section [96] such as the mass per length M_L and the cross-section radius of gyration $R_{\mathrm{CS},g}$. $R_{\mathrm{CS},g}$ is given by [96]

$$\overline{R}_{\mathrm{CS},g} = \left[\frac{\int_0^\infty r^2 \tilde{p}_{\mathrm{CS}}(r)\, dr}{2\int_0^\infty \tilde{p}_{\mathrm{CS}}(r)\, dr} \right]^{1/2} \tag{13}$$

and the cross-section forward scattered intensity $I_{\mathrm{CS}}(0)$ by

$$I_{\mathrm{CS}}(0) = 2\pi \int_0^\infty \tilde{p}_{\mathrm{CS}}(r)\, dr. \tag{14}$$

M_L (in units g/cm) can be calculated via

$$M_L = \frac{I_{\mathrm{CS}}(0)}{\Delta\rho_m^2}. \tag{15}$$

The resulting values are summarized in Table I.

We see that an exchange of H_2O with D_2O results in a decrease of approximately 15% of $I_{\mathrm{CS}}(0)$ due to the lower values of the scattering length density for a subunit of one lecithin and two water molecules ($\Delta\rho_m = -5.87 \times 10^{10}$ cm/g for H_2O and $\Delta\rho_m = -5.53 \times 10^{10}$ cm/g for D_2O), whereas the cross-section radius of gyration increases by approximately 5% due to the higher weighting of the surfactant shell.

1. Scattering length density profile

In addition to the evaluation of the integral parameters of the micellar cross section, we can also aim at a quantitative estimate of the radial scattering length density profile $\Delta\rho(r)$. This can be done by a deconvolution of the pair distribution function $\tilde{p}_{\mathrm{CS}}$ using the square-root deconvolution method [66,93]. For the semidilute sample ($w_0 = 2.0$, $c = 16$ mg/ml) the resulting profile $\Delta\rho(r)$ versus r is shown in Fig. 4(d). The distance distribution function $\tilde{p}_{\mathrm{CS}}(r)$ obtained via the IFT and the fitted one by using the deconvoluted scattering length density distribution are shown in Fig. 4(c). Within the fit range $12\ \text{Å} < r < 55\ \text{Å}$, both functions are in good agreement. The range is limited at short distances by diffuse longitudinal correlations [66].

Following this deconvolution procedure we have now access to the cross-section profile on an absolute scale [in units cm^{-2}, Fig. 4(d)], which can be compared with a simple geometrical model of a tubular cross section [67]. The IFT

method has yielded a value of $M_L = 1.52 \times 10^{-13}$ g/cm (see Table I). Together with the molar mass of a ''monomer'' (one lecithin plus two water molecules) of $M_1 = 812$ g/mol, this results in a linear monomer number density of $\lambda_L = 1.13$ Å^{-1} (lecithin molecules per angstrom) along the micellar contour. The surface area per lecithin headgroup a_0 at the hydrocarbon-chain–water interface for long-chain phosphatidylcholine molecules in a variety of different aggregate structures is approximately $a_0 \approx 70$ Å^2 [4,97], which together with λ_L allows us to estimate the circumference of the cylindrical cross section at the hydrocarbon-chain–water interface $\lambda_L a_0 \approx 79.1$ Å. From the known circumference of the cylindrical cross section at the hydrocarbon-chain–water interface we can then finally calculate the inner core radius (water plus lecithin headgroup) $R_{\text{core}} \approx \lambda_L a_0 / 2\pi \approx 12.6$ Å. For the given distribution of fatty acid chain lengths in soybean lecithin the chains should extend on average over a length of approximately $l_c \approx 17$ Å. Due to the penetration of the solvent (deuterated isooctane) into the radially extended lecithin tails, a sharp steplike scattering length density profile is clearly an oversimplification. A more realistic geometrical model for a ''hairy'' cylinder [66,67] would predict that the profile should decay in a first approximation with $\Delta\rho(r) \approx \Delta\rho^{\text{tail}} R_{\text{core}}/r$ from $r_1 = R_{\text{core}}$ to $r_2 = R_{\text{core}} + l_c$. Finally, the lecithin chains can extend by approximately 5–6 Å beyond l_c [6], i.e., $\Delta\rho(r) = 0$ should occur at $r \approx 35$ Å.

Figure 4(d) reveals that the experimentally obtained excess scattering length density profiles $\Delta\rho(r)$ are in close agreement with the expectation based on the simple geometrical model. We not only recover the predicted cross-section dimensions of the tubular micelles, but the magnitudes of the experimentally determined values of $\Delta\rho(r)$ agree on an absolute scale to within 10–20 % with the predictions based on the known chemical composition of the polar core (water plus lecithin headgroup) and the apolar shell (lecithin tail).

It is only the predicted very strong variations of $\Delta\rho(r)$ between the water core and headgroup region that we do not observe. However, this is not surprising as for these very low values we do not expect to find a clear separation between the water core and headgroup region but rather a quite extended water distribution throughout the inner part of the micellar core, with an average value of $\Delta\rho_m(r) = -5.83 \times 10^{10}$ cm/g for H_2O and $\Delta\rho_m(r) = -4.50 \times 10^{10}$ cm/g for D_2O contrast. This modified model cross section does indeed agree very well with the results from SQDEC and we find deviations of less than 10% on an absolute scale.

2. Integral parameters and their dependence on solution composition

After having established the local tubular cross-section structure through the combination of contrast variation experiments and an analysis using IFT and SQDEC, we investigate the w_0 dependence of the integral parameters describing local structure (M_L, $R_{\text{CS},g}$), which will be incorporated in the final attempt to calculate the full structure factor $S(q,c)$. The distance distribution function $\tilde{p}_{\text{CS}}(r)$, the cross-section scattering intensity $I_{\text{sc}}(0)$, and the radius of gyration of the cylindrical cross-section $R_{\text{CS},g}$ were determined for different dilution series by IFT under identical conditions, such as the cutoff limit $q_{\min} = 0.04$ Å^{-1}, as discussed before.

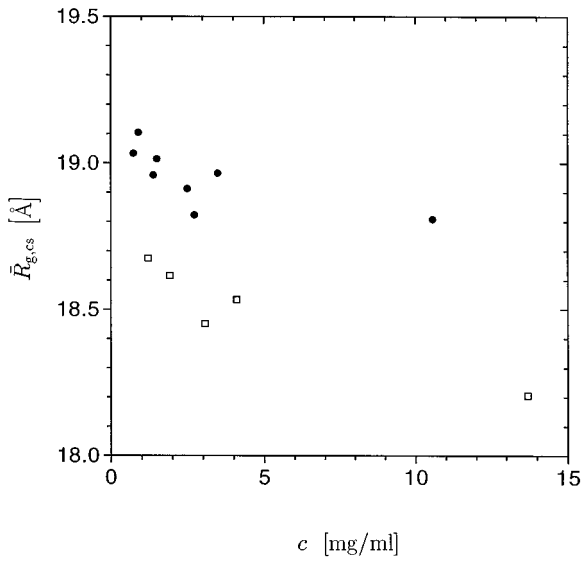

FIG. 5. Cross-section radius of gyration $\overline{R_{g,\text{CS}}}$ versus lecithin concentration c for two different water-to-lecithin ratios: $w_0 = 1.5$ (□) and $w_0 = 2.5$ (●).

Based on Eq. (13), we calculated the cross-section radii of gyration shown in Fig. 5. With increasing water content (from $w_0 = 1.5$ to 2.5) one observes a small increase of the cross-section radius of gyration in the range of approximately 0.5 Å due to the increasing amount of water in the tubular reverse micelles, whereas the concentration dependence of $R_{\text{CS},g}$ for a given water content w_0 primarily reflects the influence of interaction effects. Such contributions become more dominant at higher concentrations, which is indicated in the slightly larger error bars of the IFT fits with increasing concentration. The calculated mass per length of the stock solutions results in $M_L = 1.42 \times 10^{-13}$ g/cm for $w_0 = 1.5$ and $M_L = 1.55 \times 10^{-13}$ g/cm for $w_0 = 2.5$.

Although the IFT uses the assumption that the cross-section contribution to the total scattering can be decoupled from the rest, it has the advantage that it does not rely on the low-q part of the data used in the model fitting approach and that no specific model assumptions have to be made regarding the overall size distribution and overall structure of the micelles. Therefore, contributions from polydispersity and interaction effects are minimized, which should result in a more reliable determination of integral parameters $R_{\text{CS},g}$ and M_L at finite concentrations for different water-to-lecithin ratios.

This is supported, for example, by the data shown in Fig. 5, which demonstrates that interaction effects do result in a decrease of $R_{\text{CS},g}$ by less than 3% even at concentrations of approximately three times c^*. In combination with the deconvoluted scattering length density profiles discussed in Sec. III C 1, we can profit from the very accurate measurements of both the scattering length density profiles and the integral parameters in order to measure and verify the actual surfactant concentrations. From several series of SANS measurements performed with different stock solutions we know that the local arrangement (e.g., water channel surrounded by

a lecithin monolayer) of wormlike lecithin micelles in deuterated isooctane does not change with concentration. Therefore, the distance distribution functions and excess scattering length density profiles, respectively, should coincide on an absolute scale for all concentrations. Any deviations between samples with the same value of w_0, which do not show differences in $R_{CS,g}$, can thus be attributed to uncertainties in the concentration. The SANS data on an absolute scale can therefore be used to check and correct the actual concentration in samples prepared by dilution from stock solutions. The preparation of highly diluted samples can in fact realistically be done by using dilutions from concentrated stock solutions only since the small values of w_0 cannot be achieved directly for small sample volumes and low concentrations with sufficient precision. The preparation of larger samples cannot be considered as a practical solution due to the requirement to use the prohibitively expensive deuterated isooctane. While dilution from a stock solution is generally no problem for lower values of w_0, considerable uncertainties arise due to the strongly viscoelastic nature of samples with $w_0 \geq 2.5$, where giant micelles form already at very low concentrations. Therefore, we have cross-checked the concentration in all samples by performing an IFT analysis on an absolute scale and all concentrations used have been corrected in this way.

D. Data analysis: Flexibility and overall structure

After having analyzed the local structure of the lecithin reverse micelles in deuterated isooctane we are now in a position to investigate the intermediate-q range of the scattered intensity. We will explicitly use the information obtained by IFT and SQDEC techniques on local length scales to reduce the number of adjustable parameters in a nonlinear least-squares fitting procedure based on a model cross section for a single chain with excluded-volume effects [63]. In this section we aim at a quantitative evaluation of the flexibility, which is given in terms of either the persistence length l_p or Kuhn length b, where $b=2l_p$.

The starting point of our discussion is Fig. 6, which shows the scattered intensity for two samples with different water-to-lecithin ratios ($w_0=1.5$ and 2.5) in the so-called bending rod or Holtzer plot given by $qI(q)$ versus q [51,98,99]. This representation provides a sensitive way to test the agreement between theoretical and experimental scattered intensity for semiflexible chains as it significantly amplifies all deviations between data and theoretical curve. For semiflexible polymers, the Holtzer plot visualizes the distinct scaling regions discussed already in a previous section. Special emphasis is given thereby to the crossover from polymerlike to rodlike behavior, which shows up as a distinct plateau due to the characteristic q^{-1}-scattering pattern of an infinitely thin cylinder. Such a plateau can easily be recognized in the intermediate-q range of the data presented in Fig. 6. Towards higher q, a decay in the scattered intensity occurs because of the finite cross section that extends into the rodlike region. At lower scattering vectors we clearly see an upturn due to the flexible coil-like structure of the wormlike micelles on length scales larger than l_p.

In contrast to the physical properties on local length scales that are not significantly influenced by interaction effects (as shown in Sec. III C), the situation appears to be more complicated on intermediate length scales. The evaluation of the scattered intensity is hindered by the fact that a clear distinction between the intrinsic stiffness and interaction effects is difficult to achieve. Even without interactions, the precise determination of the flexibility would cause problems because the often-used crossover relationships or asymptotic expansions from the coil or rod limit are too uncertain to provide a good estimate of the persistence length.

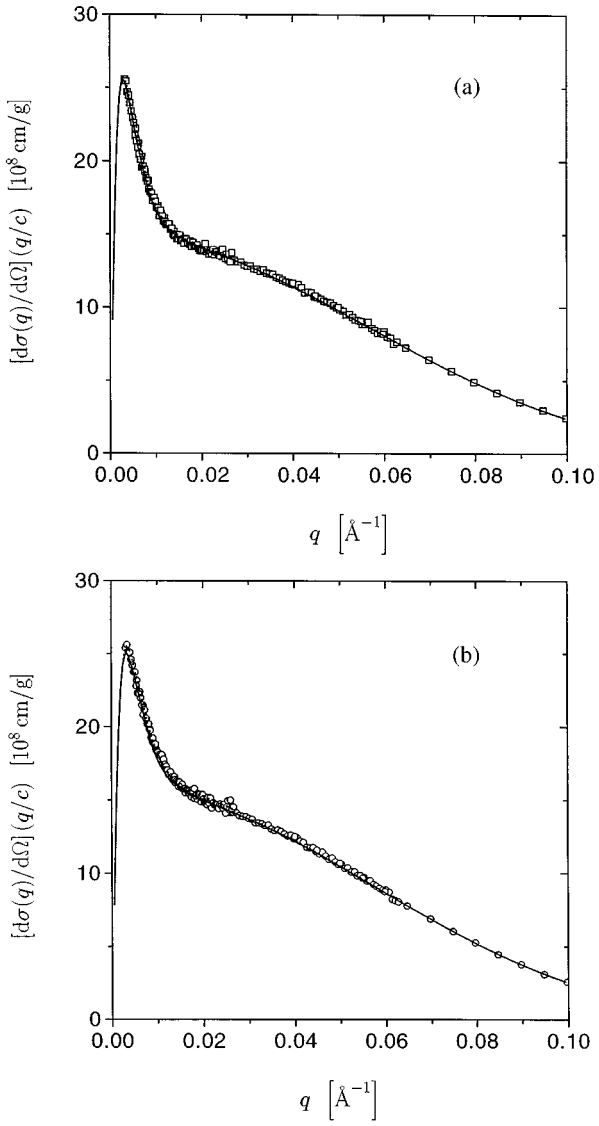

FIG. 6. Comparison of experimental data for wormlike micelles (□, $w_0=1.5$; ○, $w_0=2.5$) with theoretical curves based upon a least-squares fitting procedure of a single-chain scattering function with excluded-volume effects in the Holtzer representation. (a) $w_0=1.5$ with $c=2.09$ mg/ml and (b) $w_0=2.5$ with $c=1.64$ mg/ml.

In order to overcome these problems, an extensive Monte Carlo simulation study was performed [59] that aimed to determine a suitable model cross section that could be applied in a least-squares analysis of real wormlike micelles [63]. The model used in the simulations is a discrete representation of a Kratky-Porod wormlike chain model with excluded-volume interactions applied in the pseudocontinuous limit. From the simulations scattering functions were

generated for various ratios of contour length L to Kuhn length b and a parametrized expression was derived of the form

$$S_{\mathrm{WC}}(q,L,b)=\{[1-\chi(q,L,b)]S_{\mathrm{chain}}(q,L,b) + \chi(q,L,b)S_{\mathrm{rod}}(q,L)\}\Gamma(q,L,b), \quad (16)$$

where $S_{\mathrm{chain}}(q,L,b)$ is the scattering function of a flexible chain with excluded-volume effects, $S_{\mathrm{rod}}(q,L)$ is the scattering function of a rod, $\chi(q,L,b)$ is a crossover function, and the function $\Gamma(q,L,b)$ corrects the crossover region. Numerical approximations to these functions have been determined and these provide interpolations between the simulated functions [63].

Within the decoupling approximation, the finite size of the local cross section is included in a separate scattering function of a simplified two-shell cross section. The applicability of this model is supported by the scattering length density profile, which we have obtained independently with IFT and SQDEC methods [Fig. 4(d)]. The cross-section scattering function $S_{\mathrm{CS}}(q)$ for the locally cylindrical micelles is given by a core and shell model

$$S_{\mathrm{CS}}(q)=\frac{\left[\rho_2\pi R_2^2 2\frac{J_1(qR_2)}{qR_2}+(\rho_1-\rho_2)\pi R_1^2 2\frac{J_1(qR_1)}{qR_1}\right]^2}{[\rho_2\pi R_2^2+(\rho_1-\rho_2)\pi R_1^2]^2}, \quad (17)$$

where $J_1(x)$ is the Bessel function of first order, R_1 and R_2 are the core radius and the outer cylinder radius, and ρ_1 and ρ_2 are the scattering length density of the core and the outer shell.

It is known from previous SLS [54] and SANS [39] experiments that size polydispersity has to be included due to the equilibrium nature of the micelle. The scattering function S_{WC} of polydisperse wormlike micelles is given as the z average

$$\langle S_{\mathrm{WC}}(q,L,b)\rangle_z=\frac{\int N(L)L^2 S_{\mathrm{WC}}(q,L,b)dL}{\int N(L)L^2 dL}, \quad (18)$$

where $N(L)$ is the number distribution of wormlike chains with contour length L and $S_{\mathrm{WC}}(q,L,b)$ is the normalized scattering function given by Eq. (16). In our data analysis we apply the Schulz-Zimm distribution [84,85] and the polydispersity is fixed to $\langle M\rangle_w/\langle M\rangle_n=2$ [9].

A typical fit procedure involves the optimization of seven parameters. Five of them are determined by the high-q part of the data and were obtained from an independently performed analysis of the local properties with the help of IFT and SQDEC techniques. On the local length scale we have the inner and outer radii of the cylindrical cross section (R_1,R_2), the mass per length (M_L), the ratio of the scattering length densities of inner and outer core (ρ_1/ρ_2), and the background. On the intermediate and global scale we have the persistence length l_p and the contour length L. As mentioned before, we have fixed the polydispersity to the probable value $\langle M\rangle_w/\langle M\rangle_n=2$. In the first step of our analysis we check and optimize the input values of the local physical parameters via a grid search; after that we continue the least-squares analysis with all parameters until the fitting procedure converges. As shown in Fig. 6, the resulting fit based on this procedure provides an excellent description of the experimental data.

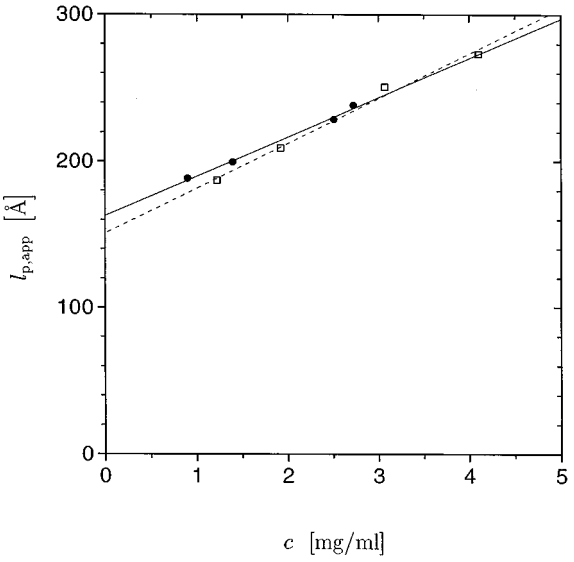

FIG. 7. Apparent persistence length $l_{p,\mathrm{app}}$ versus concentration for $w_0=1.5$ (□) and $w_0=2.5$ (●). In the limit of $c\to 0$ the linear fits result in $l_p\approx 150$–160 Å.

In the next step we performed the analysis for samples with different concentrations. The resulting (apparent) persistence lengths $l_{p,\mathrm{app}}$ for $w_0=1.5$ and 2.5 are shown in Fig. 7. We have restricted our investigation of the concentration dependence to samples that were prepared by diluting the same stock solution. Furthermore, the actual concentration values were checked via the calculated M_L as described above.

For each data set with the same water-to-lecithin ratio we have chosen the same fit range. For $w_0=1.5$ we have taken $q_{\min}=8\times10^{-3}$ Å^{-1}; for $w_0=2.5$ the lower boundary was $q_{\min}=2.3\times10^{-3}$ Å^{-1}. As a result, we can see that the calculated persistence length depends linearly on concentration. This finding is due to the fact that we apply in our analysis a least-squares fitting procedure based on the single coil scattering function where interaction effects are neglected. In order to estimate the true persistence length we have to make an extrapolation to $c\to 0$. In this limit we find that $l_p\approx 150$ Å for $w_0=1.5$ and $l_p\approx 160$ Å for $w_0=2.5$.

Results from a many-chain Monte Carlo simulation study [68] of the wormlike chain model have indeed demonstrated that interaction effects do influence the structure factor even in the q region used to determine l_p. In this study, a series of static structure factors at concentrations below and above c^* was generated and analyzed using the same fit function for single coils as for the analysis of the data from lecithin reverse micelles [Eq. (16)]. A distinct concentration dependence of $l_{p,\mathrm{app}}$ was also found. A careful analysis of the conformation statistics (bond angle correlation function) of the individual chains generated in the simulation clearly revealed that the change in $l_{p,\mathrm{app}}$ with concentration is not a result of a change in the intrinsic chain flexibility but a struc-

ture factor effect on a relatively local scale. Having eliminated the effects of finite concentrations on $l_{p,\mathrm{app}}$, we are able to provide precise values for the persistence length of a micelle. Moreover, our results clearly demonstrate that estimates made from single measurements at finite concentrations or using crossover relations can only be used with caution.

1. Concentration dependence of the static correlation length

Based on the detailed data analysis presented so far, we have values for M_L, l_p (or b), and quantitative relations to calculate the actual weight-average molar mass $\langle M\rangle_w$, the reduced concentration X, and the static structure factor in the limit $q\rightarrow 0$, $S(0)$, for any given surfactant concentration for lecithin in deuterated isooctane at $w_0=1.5$. This means that we not only have the molar mass as a measure of the micellar size, but that we can also calculate structural parameters such as the weight-average contour length $\langle L\rangle_w$ or the mean-square radius of the gyration $\overline{R_{g,0}}$ of the micelles in the hypothetical case of no interactions for any value of c. We are thus in a good position to tackle our ultimate goal, i.e., to try to calculate the full structure factor $S(q,c)$ using appropriate models from polymer physics. In a first step we can see whether the initial decay of the reduced scattering intensity is indeed compatible with our combined results from SLS (Fig. 3) and SANS (M_L,b).

The basis for this is the existence of a universal relation between ξ_s and X for polymers in good solvents, which can be written as

$$\frac{\xi_s}{\overline{R}_{g,0}}=F_s(X), \tag{19}$$

where $\overline{R_{g,0}}$ is the radius of gyration that the polymer would have in the limit $c\rightarrow 0$. Experiments with polystyrene of different molar mass in good solvents have indeed demonstrated that such a universal curve $F_s(X)$ can be constructed that shows no systematic dependence on the molar mass or the solvent [100]. Attempts have been made to put this finding onto a solid theoretical basis, and an explicit functional form for $F_s(X)$ has, for example, been calculated with renormalization-group methods [101]. However, whereas the theoretical calculations reproduce the correct shape of the experimental master curve, the calculated crossover occurs at a too-small value of X and results in a strongly overestimated effect of concentration on ξ_s [87].

We can now try to generate such a universal curve from our experimental results. On the basis of the known local structure of the lecithin reverse micelles ($w_0=1.5$ and 2.5) and the relation between the micellar contour length L, the weight-average molar mass $\langle M\rangle_w$, and M_L given by $\langle L\rangle_w=\langle M\rangle_w/N_AM_L$, the theoretical values of $R_{g,0}(c)$ can then be calculated for all values of c investigated. This is done using the relation between the radius of gyration $\overline{R_{g,0}}$, the contour length L, the persistence length l_p for wormlike chains without excluded-volume effects [102]

$$\overline{R^2_{g,0}}(L,l_p)=\frac{Ll_p}{3}\left(1-\frac{3}{2N_K}+\frac{3}{2N_K^2}-\frac{3}{4N_K^3}\left[1-e^{-2N_K}\right]\right), \tag{20}$$

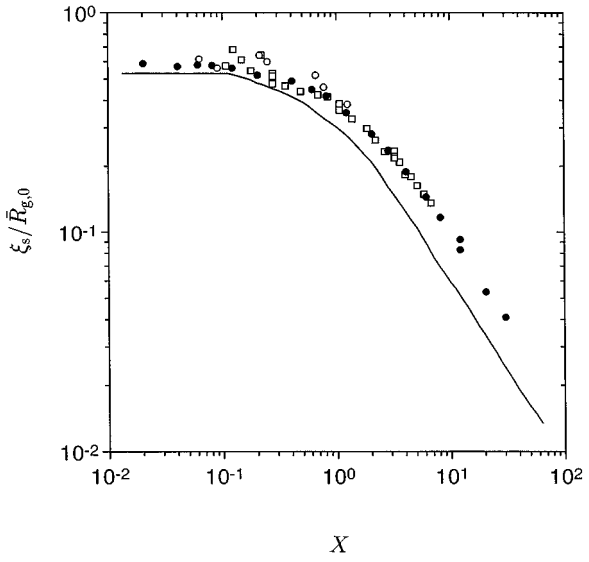

FIG. 8. Comparison of $\xi_s/\overline{R_{g,0}}$ versus reduced concentration X for lecithin wormlike micelles in deuterated isooctane with $w_0=1.5$ (□), $w_0=2.5$ (○), and Monte Carlo simulations [68] with a ratio of $L/b=90$ (●), where L is the contour length and b the Kuhn length. The theoretical curve according to the renormalization-group theory is shown as a solid line.

where $N_K=L/b$ is the number of Kuhn length $b=2l_p$ per contour length, and the expansion factor α_s, which accounts for the effect of excluded volume in so-called good solvents through

$$\overline{R_g^2}=\alpha_s^2(N_K)\overline{R^2_{g,0}}. \tag{21}$$

As derived from a systematic study of the conformation of wormlike micelles with excluded-volume effects by Monte Carlo simulations, the expansion factor α_s follows the equation [59]

$$\alpha_s^2(N_K)=\left[1+\left(\frac{N_K}{3.12}\right)^2+\left(\frac{N_K}{8.67}\right)^3\right]^{\epsilon/3} \tag{22}$$

where $\epsilon=0.17$.

Based on the set of equations (9), (10), (20), (21), and (22), we can thus calculate the expected values of the ''ideal'' radius of gyration of the micelles and the corresponding values of the reduced concentration X for all concentrations investigated at the water-to-lecithin ratio of $w_0=1.5$. Together with the experimental values of the static correlation length determined from the initial q dependence of the scattered intensity as described in Sec. II, we can construct a curve $\xi_s/R_{g,0}$ versus X as given in Fig. 8. A similar analysis can also be performed for all the data obtained with $w_0=2.5$. We see that all data points collapse nicely onto a single master curve, which shows the same functional form as the renormalization-group prediction shown as the solid line in Fig. 8. When compared with the situation encountered in polymers, we find a similar systematic difference between the experimental and theoretical curves. In view of the unsatisfactory theoretical basis, a systematic Monte Carlo simulation study of wormlike chains with excluded-volume interactions at different concentra-

tions ranging from very dilute to well above the overlap threshold was started [68]. The simulations were based on our previous Monte Carlo studies of single-chain properties using a Kratky-Porod model with fixed valence angles and free rotations about the bonds, where the strength of the excluded-volume interactions and the Kuhn length as a measure of the chain flexibility were chosen so as to closely mimic wormlike micelles or polystyrene in good solvents [59,63]. Simulations were made for several ratios of contour length to Kuhn length L/b using a box with periodic boundary conditions. During these simulations, the scattering function [103] as well as the radius of gyration of the chains was calculated and sampled as described elsewhere [68].

The thus calculated scattering functions $d\sigma(q)/d\Omega$ was analyzed and quantities such as the forward scattering and the correlation length could be obtained from the initial part of $d\sigma(q)/d\Omega$ as a function of concentration. Moreover, from the initial part of the concentration dependence of $d\sigma(0)/d\Omega$ the product of $A_2\langle M\rangle_w c$ was determined, which allowed us to calculate the reduced concentration X for all ratios L/b and volume fractions simulated. Having determined these quantities, we could then construct curves $S(0)$ versus X and $\xi_s/R_{g,0}$ versus X from the simulation results. We found that for both reduced quantities all the simulation data for different chain lengths fall onto single master curves, in good agreement with the experimental data for polystyrene in good solvents. The simulation results will be described in full details elsewhere [68].

An example of the resulting curve $\xi_s/R_{g,0}$ versus X from the Monte Carlo simulations for $L/b=90$ is given in Fig. 8 as the filled circles. We see that the calculated data points from the light scattering measurements with lecithin reverse micelles and the simulation data perfectly agree. The simulations thus strongly support our findings from the renormalization-group analysis of the forward scattering intensity and provide us with a very valuable consistency test. It is important to point out that in this comparison no free parameters other than the previously determined values of B_1, B_2, α, l_p, and M_L for lecithin reverse micelles were used. Moreover, the agreement between the concentration dependence of the reduced correlation length $\xi_s/R_{g,0}$ from Monte Carlo simulations and experimental data indicates that not only can we account for the static structure factor in the limit $q\to 0$ by using renormalization-group theory, but we can also reproduce the initial q dependence of $S(q,c)$ for polymerlike micelles. In a final step we can now try to use the full structure factor $S(q,c)$ estimated from Monte Carlo simulations in order to analyze the experimental data from the lecithin reverse micelles.

2. Modified random-phase approximation

The basis for this final step is the finding that all structure factors obtained by the Monte Carlo simulations can be reproduced by using a phenomenological ansatz taken from the random-phase approximation (RPA) frequently used in polymer physics. A theoretical treatment of the elastic coherent scattering intensity for a polymer solution at arbitrary concentration leads to an expression of the form

$$\frac{d\sigma}{d\Omega}(q,c)=Kc\langle M\rangle_w S_{\mathrm{RPA}}(q,c), \tag{23}$$

with

$$S_{\mathrm{RPA}}(q,c)=\frac{S(q)}{1+v(c)S(q)}, \tag{24}$$

which is consistent with the random-phase approximation [104]. K is the contrast factor for either SLS or SANS and $S(q)$ denotes the normalized single-particle scattering function. In this approximation $v(c)$ is a concentration-dependent excluded-volume parameter that has been introduced to incorporate many chain interactions. Unfortunately, to our knowledge, there exists no quantitative treatment that would allow us to incorporate the effect of molar mass into $v(c)$ and we thus have no means to calculate $v(c)$ as a function of concentration, contour length, and flexibility. Moreover, most theoretical treatments have been based on a model for either flexible chains or rigid rods. An analysis of the static structure factor generated in the Monte Carlo simulations [68] has led to the discovery that a simple RPA expression of the form of Eq. (24) leads to systematic deviations at higher values of q when using the single-chain scattering function for wormlike chains with excluded-volume effects as derived from the Monte Carlo results presented recently [63]. However, good agreement for all values of q was obtained when using a phenomenological derivative of the original RPA expression

$$S_{\mathrm{RPA}}(q,c)=\frac{S_{\mathrm{WC}}(q)}{1+\dfrac{1-S(0)}{S(0)}\,f_{\mathrm{Debye}}(q^2\overline{R_g^2})}, \tag{25}$$

where $S_{\mathrm{WC}}(q)$ is the single-chain scattering function for a wormlike chain with excluded-volume effects according to Eq. (16) and

$$f_{\mathrm{Debye}}(x)=2\,\frac{e^{-x}-1+x}{x^2} \tag{26}$$

is the Debye function, i.e., the form factor of a Gaussian chain. The factor $[1-S(0)]/S(0)$ ensures the correct value of $S_{\mathrm{RPA}}(q=0,c)$ when using Eq. (8) for $S(0)$. Due to the very good agreement between the initial q dependence of $S(q,c)$ obtained from the Monte Carlo simulations and the calculated relation between $\xi_s/R_{g,0}$ and X for lecithin reverse micelles as demonstrated in Fig. 8, we can hope that the phenomenological expression given in Eq. (25) could provide a quantitative description of the experimental scattering data at all values of q. We have therefore used an *ad hoc* modification of Eq. (25) of the form [95]

$$S_{\mathrm{RPA}}(q,c)=\frac{\langle S_{\mathrm{WC}}(q)\rangle_z S_{\mathrm{CS}}(q)}{1+\dfrac{1-S(0)}{S(0)}\,f_{\mathrm{Debye}}(q^2\overline{R_g^2})} \tag{27}$$

in order to calculate the normalized intensity of a solution of lecithin in deuterated isooctane for $w_0=2.5$ with c

$=3.49$ mg/ml, i.e., at a concentration close to c^*. From an analysis of the concentration dependence of the apparent molar mass for $w_0=2.5$ we have obtained values of B_1, B_2, and α, which we can use to calculate the weight-average molar mass $\langle M\rangle_w=2.9\times10^7$ g/mol of the micelles at this concentration [Eq. (9)], and the expected value of the reduced concentration $X=1.26$ [Eq. (10)] or the corresponding value of $S(0)=0.365$ [Eq. (8)].

In combination with the experimentally determined value of M_L we obtain the weight-average contour length $\langle L\rangle_w=36\,000$ Å. Together with the experimentally determined value of $l_p=160$ Å (Fig. 7) and the cross-section radius of gyration $R_{CS,g}=19$ Å as obtained from the entire series of SANS measurements (Fig. 5), we now have all the parameters required in an attempt to calculate the full structure factor on an absolute scale using Eq. (27). The result of this calculation is shown in Fig. 9(a) together with the experimental data from light and neutron scattering experiments and a calculation for the ideal scattering curve using the single coil scattering function without interaction effects. We find excellent agreement over the entire range of q values, which spans more than three orders of magnitude. In particular, the intermediate-q range around the crossover from flexible coil to stiff cylinder, for which no previous theoretical description existed, is remarkably well reproduced. This is shown in more detail in Fig. 9(b) using a Holtzer plot. The agreement between calculated curve and experimental data is generally well below 10%, with a maximum deviation of around 13% in the crossover region.

It is important to point out that the only parameters used in the calculation were integral parameters obtained from a combined analysis of a large set of measurements such as the growth parameters α, B_1, and B_2 as predicted from an analysis of all the light scattering data, the flexibility as determined from a set of SANS measurements in the intermediate-q range, and M_L and $R_{CS,g}$ as determined from a concentrated stock solution. No attempts to adjust or fit some of these quantities to the individual data set for $c=3.49$ mg/ml have been made. The close correspondence between calculation and experimental data is thus quite remarkable as it is performed on an absolute scale and relies on the perfect agreement between the light scattering and the SANS data. In fact, some of the discrepancy between data and the calculated curve may come from a slight mismatch that leads to systematically too-high values of the calculated intensity when compared to the SANS data. Another point where we still need improvement is the correct treatment of polydispersity. The expression for $S(q,c)$ given in Eq. (25) has been derived from Monte Carlo simulations of monodisperse chains, whereas micelles are known to be very polydisperse with an exponential size distribution described by the Schulz-Zimm distribution according to Eq. (7) with $\langle M\rangle_w/\langle M\rangle_n=2$. In order to incorporate polydispersity we have chosen an *ad hoc* treatment in which we calculate the appropriate intensity-weighted polydisperse single-chain scattering function using the Schulz-Zimm distribution, whereas we used the weight-average contour length to calculate the corresponding Debye function and the $S(0)$ from the renormalization-group theory analysis, i.e., we relied on some sort of decoupling approximation. We do not really have a theoretical justification for this procedure other than the fact that the result was very encouraging and it is clear that we desperately need a better understanding of the effects of polydispersity.

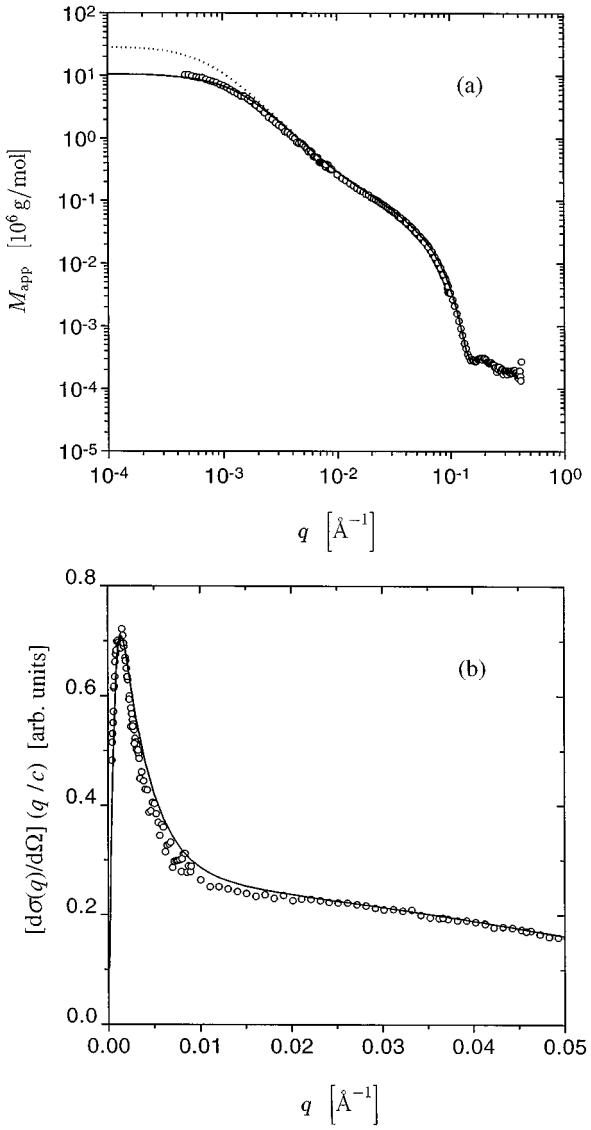

FIG. 9. Comparison of experimental data for lecithin wormlike micelles ($w_0=2.5$, $c=3.49$ mg/ml) with theoretical results based on the single-chain scattering function with excluded-volume effects (dotted line) and the modified random-phase approximation (straight line). For details see the text. (a) Full scattering curve over an extended q range of approximately three decades in q. (b) Representation in a so-called bending rod or Holtzer plot.

IV. CONCLUSION

The static and dynamic properties of ''equilibrium polymers'' have been the subject of numerous theoretical and experimental studies. In particular, surfactant systems in which giant wormlike micelles are formed frequently have been used as very interesting model systems. The presence of flexible and locally cylindrical aggregates and the close analogy between the structural properties of wormlike micelles and polymers have been demonstrated in a large variety of

systems primarily by scattering experiments. However, despite the considerable effort devoted to a characterization of polymerlike micelles and microemulsions, we still lack precise knowledge of fundamental properties, such as the concentration-dependent micellar growth or the micellar flexibility, and the available data are inconsistent. A major obstacle in experimental studies employing scattering methods has always been the problem of how to incorporate growth, polydispersity, flexibility, and intermicellar interactions in a consistent way in the interpretation of scattering data. A first step in this direction was made recently, where it was shown that one can successfully tackle this problem by directly applying the results from conformation space renormalization-group theory for semidilute polymer solutions to equilibrium polymers. However, we cannot expect that a direct application of renormalization-group theory can yield a quantitative description of the static structure factor on all length scales, which could otherwise be used as an additional test of these earlier findings.

Additional important progress towards a full description of $S(q,c)$ was recently made by using Monte Carlo simulations of wormlike chains with excluded-volume effects in the pseudocontinuous limit, which provided accurate expressions for the single coil scattering function on all length scales. As demonstrated in this article, these parametrized scattering functions are capable of fitting the experimental data from polymerlike reverse micelles over more than three decades in q with very good agreement. The use of numerical expressions for the full scattering function allows for an incorporation of polydispersity and permits us to determine apparent values of the contour length and the persistence length with high precision. These accurate values for $l_{p,\mathrm{app}}$ yield clear evidence that the SANS data at intermediate q, from where we extract the information on the persistence length, is influenced by intermicellar interaction effects even at relatively low concentrations $c<c^*$. It is only from a direct comparison with a recent Monte Carlo simulation study of many chain systems that we are able to identify and eliminate the interaction effects and provide precise values for the persistence length of wormlike micelles and microemulsions. These findings now open new opportunities to study micellar flexibility and investigate the influence of compositional changes, temperature, or charges on l_p.

A direct comparison of experimental data and a calculated full structure factor $S(q,c)$ at arbitrary concentrations using the independently determined parameters (the ''true'' molar mass $\langle M(c)\rangle_w$, the true persistence length l_p, and the mass per length M_L) represents the ultimate consistency test for any theoretical description of micellar growth, structure, and interactions. The results presented in this article strongly suggest that a phenomenological form of $S(q,c)$ obtained from the Monte Carlo simulations indeed achieves this formidable task. It is clear that we still have to make major progress in the incorporation of polydispersity and subject the proposed expression for the static structure factor to additional test. Nevertheless, we believe that we have made an important step towards a complete description of $S(q,c)$ that fully incorporates micellar growth, flexibility, and interactions in a consistent way.

ACKNOWLEDGMENTS

We gratefully acknowledge the contributions of Carolina Cavaco during the setup of the first experiments. G.J. thanks John Daicic for his careful reading of the manuscript. This study was supported by the Swiss National Science Foundation (Grants Nos. 20-40339.94 and 20-46627.96). The neutron-scattering experiments were performed partly at the DR3 reactor at Risø National Laboratory and supported by the Commission of the European Community through the Large Installation Programme. We also gratefully acknowledge the support from the Institut Laue-Langevin in Grenoble, where part of the SANS measurements were performed on the instrument D22.

[1] S. A. Safran, L. A. Turkevich, and P. Pincus, J. Phys. (France) **45**, L69 (1984).
[2] S. A. Safran, in *Structure and Dynamics of Strongly Interacting Colloids and Supramolecular Aggregates in Solution*, edited by S. H. Chen, J. S. Huang, and P. Tartaglia (Kluwer Academic, Dordrecht, 1992).
[3] S. A. Safran, *Statistical Thermodynamics of Surfaces, Interfaces, and Membranes* (Addison-Wesley, Reading, MA, 1994).
[4] J. N. Israelachvili, D. J. Mitchell, and B. W. Ninham, J. Chem. Soc. Faraday Trans. 2 **72**, 1525 (1976).
[5] C. Tanford, *The Hydrophobic Effect*, 2nd ed. (Wiley, New York, 1980).
[6] J. N. Israelachvili, *Intermolecular and Surfaces Forces*, 2nd ed. (Academic, London, 1992).
[7] M. E. Cates, Macromolecules **20**, 2289 (1987).
[8] M. E. Cates, J. Phys. (France) **49**, 1593 (1988).
[9] M. E. Cates and S. J. Candau, J. Phys.: Condens. Matter **2**, 6869 (1990).
[10] L. Magid, in *Dynamic Light Scattering: The Method and some Applications*, edited by W. Brown (Clarendon, Oxford, 1993).
[11] P. Schurtenberger, in *Light Scattering: Principles and Development*, edited by W. Brown (Clarendon, Oxford, 1996).
[12] *Structure and Flow in Surfactant Solutions*, edited by C. A. Herb and R. K. Prud'homme (American Chemical Society, Washington, DC, 1994).
[13] F. Odijk, Curr. Opinion Colloid Interface Sci. **1**, 337 (1996).
[14] F. Lequeux, Curr. Opinion Colloid Interface Sci. **1**, 341 (1996).
[15] M. E. Cates, J. Phys.: Condens. Matter **8**, 9167 (1996).
[16] N. A. Mazer, G. B. Benedek, and M. C. Carey, J. Phys. Chem. **80**, 1075 (1976).
[17] S. J. Gravsholt, J. Colloid Interface Sci. **57**, 575 (1976).
[18] C. Y. Young, P. J. Missel, N. A. Mazer, G. B. Benedek, and M. C. Carey, J. Phys. Chem. **82**, 1375 (1978).
[19] P. J. Missel, N. A. Mazer, G. B. Benedek, C. Y. Young, and M. C. Carey, J. Phys. Chem. **84**, 1044 (1980).

[20] G. Porte, J. Appell, and Y. Poggi, J. Phys. Chem. **84**, 3105 (1980).
[21] S. Ikeda, S. Ozeki, and M.-A. Tsunoda, J. Colloid Interface Sci. **73**, 27 (1980).
[22] S. Ikeda, S. Hayashi, and T. Imae, J. Phys. Chem. **84**, 744 (1980).
[23] S. Hayashi and S. Ikeda, J. Phys. Chem. **84**, 744 (1980).
[24] J. Appell and G. Porte, J. Colloid Interface Sci. **81**, 85 (1981).
[25] G. Porte and J. Appell, J. Phys. Chem. **85**, 2511 (1981).
[26] S. Ozeki and S. Ikeda, J. Colloid Interface Sci. **87**, 424 (1982).
[27] P. J. Missel, N. A. Mazer, G. B. Benedek, and M. C. Carey, J. Phys. Chem. **87**, 1264 (1983).
[28] H. Hoffmann, H. Rehage, G. Platz, W. Schorr, H. Thurn, and W. Ulbricht, Colloid Polym. Sci. **260**, 1042 (1982).
[29] H. Hoffmann, J. Kalus, H. Thurn, and K. Ibel, Ber. Bunsenges. Phys. Chem. **87**, 1120 (1983).
[30] J. Appell and G. Porte, J. Phys. (France) **44**, L689 (1983).
[31] S. J. Candau, E. Hirsch, and R. Zana, J. Phys. (France) **45**, 1263 (1984).
[32] T. Imae and S. Ikeda, J. Colloid Interface Sci. **98**, 363 (1984).
[33] S. J. Candau, E. Hirsch, and R. Zana, J. Colloid Interface Sci. **105**, 521 (1985).
[34] U. Olsson, O. Södermann, and P. Guéring, J. Phys. Chem. **90**, 5223 (1986).
[35] D. Blankschtein, G. M. Thurston, and G. B. Benedek, J. Chem. Phys. **85**, 7268 (1986).
[36] S. J. Candau, E. Hirsch, R. Zana, and M. Adam, J. Colloid Interface Sci. **122**, 430 (1988).
[37] J. Marignan, J. Appell, P. Bassereau, G. Porte, and R. P. May, J. Phys. (France) **50**, 3553 (1989).
[38] T. Imae, Colloid Polym. Sci. **267**, 707 (1989).
[39] J. S. Pedersen, S. U. Egelhaaf, and P. Schurtenberger, J. Phys. Chem. **99**, 1299 (1995).
[40] P. Schurtenberger, C. Cavaco, F. Tiberg, and O. Regev, Langmuir **12**, 2894 (1996).
[41] Z. Zhou, Y. Georgalis, W. Liang, J. Li, R. Xu, and B. Chu, J. Colloid Interface Sci. **116**, 473 (1987).
[42] R. Scartazzini and P. L. Luisi, J. Phys. Chem. **92**, 829 (1988).
[43] P. Schurtenberger, R. Scartazzini, and P. L. Luisi, Rheol. Acta **28**, 372 (1989).
[44] P. Schurtenberger, R. Scartazzini, L. J. Magid, M. E. Leser, and P. L. Luisi, J. Phys. Chem. **94**, 3695 (1990).
[45] P. Schurtenberger, L. J. Magid, J. Penfold, and R. Heenan, Langmuir **6**, 1800 (1990).
[46] P. Schurtenberger, L. J. Magid, S. M. King, and P. Lindner, J. Phys. Chem. **95**, 4173 (1991).
[47] P. Terech, V. Schaffhauser, P. Maldivi, and J. M. Guenet, Europhys. Lett. **17**, 515 (1992).
[48] P. Terech, V. Schaffhauser, P. Maldivi, and J. M. Guenet, Langmuir **8**, 2104 (1992).
[49] Z.-J. Yu and R. D. Neumann, Langmuir **10**, 2553 (1994).
[50] D. F. Evans and H. Wennerström, *The Colloidal Domain* (VCH, New York, 1994).
[51] P. D. Butler, L. J. Magid, and J. B. Hayter, in *Structure and Flow in Surfactant Solutions* (Ref. [12]), p. 250.
[52] W. van de Sande and A. Persoons, J. Phys. Chem. **89**, 404 (1985).
[53] S. U. Egelhaaf and P. Schurtenberger, J. Phys. Chem. **98**, 8560 (1994).
[54] P. Schurtenberger and C. Cavaco, J. Phys. Chem. **98**, 5481 (1994).
[55] P. Schurtenberger and C. Cavaco, J. Phys. II **3**, 1279 (1993).
[56] P. Schurtenberger and C. Cavaco, J. Phys. II **4**, 305 (1994).
[57] R. P. Hjelm, P. Thiyagarajan, and H. Alkan-Onyuksel, J. Phys. Chem. **96**, 8653 (1992).
[58] M. A. Long, E. W. Kaler, S. P. Lee, and G. D. Wignall, J. Phys. Chem. **98**, 4402 (1994).
[59] J. S. Pedersen, M. Laso, and P. Schurtenberger, Phys. Rev. E **54**, R5917 (1996).
[60] G. Porod, Monatsh. Chem. **80**, 251 (1949).
[61] O. Kratky and G. Porod, Recl. Trav. Chim. Pays-Bas **68**, 1106 (1949).
[62] T. Yoshizaki and H. Yamakawa, Macromolecules **13**, 1518 (1980).
[63] J. S. Pedersen and P. Schurtenberger, Macromolecules **29**, 7602 (1996).
[64] P. Schurtenberger and C. Cavaco, Langmuir **10**, 100 (1994).
[65] P. Schurtenberger, L. J. Magid, P. Lindner, and P. L. Luisi, Prog. Colloid Polym. Sci. **89**, 274 (1992).
[66] J. S. Pedersen and P. Schurtenberger, J. Appl. Crystallogr. **29**, 646 (1996).
[67] P. Schurtenberger, G. Jerke, C. Cavaco, and J. S. Pedersen, Langmuir **12**, 2433 (1996).
[68] J. S. Pedersen and P. Schurtenberger (unpublished).
[69] These solutions are extremely sensitive in the preparation because of possible uptake of water, which makes a direct quantitative comparison between results obtained with different stock solutions very difficult. The reproducibility can be improved considerably if the preparation is done in a controlled atmosphere, e.g., in a glove box.
[70] P. Schurtenberger and R. C. Augusteyn, Biopolymers **31**, 1229 (1991).
[71] *The Yellow Book: Guide to the Neutron Research Facilities at the ILL*, edited by K. Ibel (ILL, Grenoble, 1994). Further information: http://www.ill.fr/d22/d22.html
[72] B. Jacrot and G. Zaccai, Biopolymers **20**, 2413 (1981).
[73] M. Ragnetti and R. C. Oberthür, Colloid Polym. Sci. **264**, 32 (1986).
[74] G. D. Wignall and F. S. Bates, J. Appl. Crystallogr. **20**, 28 (1987).
[75] J. P. Cotton, in *Neutron, X-Ray and Light Scattering: Introduction to an Investigative Tool for Colloidal and Polymeric Systems*, edited by P. Lindner and T. Zemb (North-Holland, Amsterdam, 1991).
[76] B. Bergenståhl and K. Fontell, Prog. Colloid Polym. Sci. **68**, 48 (1983).
[77] K. Shinoda, Y. Shibata, and B. Lindman, Langmuir **9**, 1254 (1993).
[78] J. S. Pedersen, D. Posselt, and K. Mortensen, J. Appl. Crystallogr. **23**, 321 (1990).
[79] J. G. Barker and J. S. Pedersen, J. Appl. Crystallogr. **28**, 105 (1995).
[80] P. R. Bevington, *Data Reduction and Error Analysis for the Physical Sciences* (McGraw-Hill, New York, 1969).
[81] Y. Oono, Adv. Chem. Phys. **61**, 301 (1985).
[82] D. L. Goodstein, *States of Matter* (Dover, New York, 1985).
[83] K. Huber and W. H. Stockmayer, Macromolecules **20**, 1400 (1987).
[84] G. V. Schulz, Z. Phys. Chem. Abt. B **43**, 25 (1939).
[85] B. H. Zimm, J. Chem. Phys. **16**, 1099 (1948).

[86] T. Ohta and Y. Oono, Phys. Lett. **89A**, 460 (1982).
[87] W. Brown and T. Nicolai, Colloid Polym. Sci. **268**, 977 (1990).
[88] E. Buhler, J. P. Munch, and S. J. Candau, J. Phys. II **5**, 765 (1995).
[89] G. Jerke and P. Schurtenberger (unpublished).
[90] T. Kato, M. Kanada, and T. Seimiya, Langmuir **11**, 1867 (1995).
[91] O. Glatter, J. Appl. Crystallogr. **10**, 415 (1977).
[92] O. Glatter, J. Appl. Crystallogr. **13**, 577 (1980).
[93] O. Glatter, J. Appl. Crystallogr. **14**, 101 (1981).
[94] When compared to the data presented in Ref. [67], one has to take into account that in the present study smearing effects are less pronounced because the wavelength resolution was chosen to be 10% instead of 18% in the previous study.
[95] $S_{WO}(q)$ and $S_{CS}(q)$ are normalized to $S(q=0)=1$.
[96] O. Glatter, in *International Tables for Crystallography. Volume C. Mathematical, Physical and Chemical Tables*, edited by A. J. C. Wilson (Kluwer Academic, Dordrecht, 1992).
[97] D. Small, *The Physical Chemistry of Lipids. From Alkanes to Phospholipids* (Plenum, New York, 1986).
[98] A. Holtzer, J. Polym. Sci. **17**, 432 (1955).
[99] P. Denkinger and W. Burchard, J. Polym. Sci. B, Polym. Phys. **29**, 589 (1991).
[100] P. Wiltzius, H. R. Haller, D. S. Cannell, and D. W. Schaefer, Phys. Rev. Lett. **51**, 1183 (1983).
[101] A. Nakanishi and T. Ohta, J. Phys. A **18**, 127 (1985).
[102] H. Benoit and P. Doty, J. Phys. Chem. **57**, 958 (1953).
[103] D. Frenkel, R. J. Vos, C. G. de Kruif, and A. Vrij, J. Chem. Phys. **84**, 4625 (1986).
[104] H. Benoit, C. Picot, and M. Benmouna, J. Polym. Sci. B, Polym. Phys. **22**, 1545 (1984).